

OPEN

Detection and Viability of Colorectal Liver Metastases After Neoadjuvant Chemotherapy

A Multiparametric PET/CT-MRI Study

Vincent Dunet, MD,* Nermin Halkic, MD,† John O. Prior, MD, PhD,‡ Anass Anaye, MD,§ Reto A. Meuli, MD,* Christine Sempoux, MD,|| Alban Denys, MD,* and Sabine Schmidt, MD*

Purpose: The aim of this study was to compare combined gadolinium-ethoxybenzyl-diethylenetriamine-pentaacetic acid (Gd-EOB-DTPA)-enhanced and diffusion-weighted (DW) MRI with IV contrast-enhanced ^{18}F -FDG PET/CT to detect and assess the viability of colorectal liver metastases (CLMs) after neoadjuvant chemotherapy (NAC).

Patients and Methods: After NAC, 45 patients with CLMs were prospectively enrolled and underwent combined Gd-EOB-DTPA-enhanced and DW-MRI and contrast-enhanced ^{18}F -FDG PET/CT. Forty patients subsequently underwent surgery based on intraoperative ultrasound, which served as the reference standard for the presence of CLMs. The number of metastases detected by each technique was then compared. In 69 resected metastases, the SUV_{mean} and SUV_{max} , mean and maximum target-to-background ratio (TBR), total lesion glycolysis, metabolic tumor volume, and mean and minimum apparent diffusion coefficient (ADC) were examined to identify correlations with the corresponding tumor viability (TV) determined from histological specimens.

Results: Intraoperative ultrasound revealed 153 CLMs, 122 of which were resected. The detection rate of MRI and contrast-enhanced ^{18}F -FDG PET/CT were similar ($P = 0.61$). The SUV_{max} and minimum ADC were negatively correlated ($r = -0.34$, $P = 0.005$) on preoperative imaging after NAC. However, TV was significantly correlated with the maximum TBR ($r = 0.33$, $P = 0.006$) and mean TBR ($r = 0.37$, $P = 0.002$), but not with the minimum ADC ($r = -0.02$, $P = 0.9$) or mean ADC ($r = 0.01$, $P = 0.9$).

Conclusions: Combined Gd-EOB-DTPA-enhanced and DW-MRI and contrast-enhanced ^{18}F -FDG PET/CT allow confident detection of CLMs, but only ^{18}F -FDG PET metrics are associated with TV after NAC.

Key Words: diffusion-weighted imaging ^{18}F -FDG PET/CT, colorectal cancer, liver metastasis

(*Clin Nucl Med* 2017;42: 258–263)

Received for publication September 19, 2016; revision accepted December 4, 2016. From the Departments of *Diagnostic and Interventional Radiology, †Visceral Surgery, and ‡Nuclear Medicine and Molecular Imaging, Lausanne University Hospital, Lausanne; §Department of Radiology, Riviera and Chablais Hospitals, Vevey; and ||Institute of Pathology, Lausanne University Hospital, Lausanne, Switzerland.

Conflicts of interest and sources of funding: This study was partially funded by Bayer Healthcare Switzerland. None of the authors are employees of Bayer Healthcare, which had no role in the data collection, results analysis, or manuscript writing.

Correspondence to: Sabine Schmidt, MD, Department of Diagnostic and Interventional Radiology, Lausanne University Hospital, Rue du Bugnon 46, CH-1003 Lausanne, Switzerland. E-mail: Sabine.Schmidt@chuv.ch.

Copyright © 2017 The Author(s). Published by Wolters Kluwer Health, Inc. This is an open-access article distributed under the terms of the Creative Commons Attribution-Non Commercial-No Derivatives License 4.0 (CCBY-NC-ND), where it is permissible to download and share the work provided it is properly cited. The work cannot be changed in any way or used commercially without permission from the journal.

ISSN: 0363-9762/17/4204-0258

DOI: 10.1097/RLU.0000000000001538

Colorectal cancer (CRC) is the third most common cancer worldwide with an annual age-standardized incidence of 20.6 new cases per 100,000 inhabitants in men and 14.3 new cases per 100,000 inhabitants per year in women, with incidences varying depending on the individual country.¹ At diagnosis, synchronous colorectal liver metastases (CLMs) are present in 15% to 25% of stage IV disease,² and up to 50% of patients with CRC will develop metachronous CLMs,³ frequently with a subsequent fatal outcome. Therefore, the resection of CLMs has a major impact on the patient's survival,^{4,5} because it is the only possibility of curative treatment. While many patients are poor candidates for liver surgery due to the high number and/or localization of the nodules, preoperative combined chemotherapy regimens have been developed during the last decades. Neoadjuvant chemotherapy (NAC) has gained importance in the management of synchronous and/or metachronous CLMs to reduce the number and size of lesions, enabling resection.^{6,7}

Gadolinium-ethoxybenzyl-diethylenetriamine-pentaacetic acid (Gd-EOB-DTPA)-enhanced liver MRI has improved the detection of CLMs without a cost increase compared with MRI with extracellular contrast media.⁸ Moreover, recent studies indicated that combined Gd-EOB-DTPA-enhanced and diffusion-weighted (DW) MRI improves the detection of CLMs after NAC^{9,10} versus the use of the hepatobiliary contrast agent alone.¹¹ In addition to morphological assessment, ^{18}F -FDG PET/CT can be used to evaluate the metabolic response of CLMs, which is correlated with the histopathological response¹² and indicates a good prognosis in patients receiving NAC.^{13,14} However, to date, no study has investigated the ability of combined Gd-EOB-DTPA-enhanced and DW-MRI to assess the viability of CLMs after NAC in comparison with IV contrast-enhanced ^{18}F -FDG PET/CT.

The purpose of this prospective study was to compare the value of combined Gd-EOB-DTPA-enhanced and DW-MRI with IV contrast-enhanced ^{18}F -FDG PET/CT for the detection of CLMs and to assess their residual viability after NAC, using histology and intraoperative ultrasound (US) as reference standards.

PATIENTS AND METHODS

Study Design and Population

Between July 2010 and September 2015, 45 patients (mean age, 63 ± 10 years; 29 men [64%]) with CLMs were prospectively enrolled after NAC treatment. Everyone was examined by combined Gd-EOB-DTPA-enhanced (EOB Primovist; Bayer, Germany) and DW-MRI as well as IV contrast-enhanced ^{18}F -FDG PET/CT. Inclusion criteria were age older than 18 years and unresectable CLMs before NAC. Exclusion criteria were as follows: unresectable CLMs

after NAC, contraindication to MRI (claustrophobia, renal failure with an estimated GFR <30 mL/min, pacemaker), contraindication to iodine contrast (renal failure with estimated GFR <30 mL/min, anaphylaxis). The resectability of the CLMs was established by consensus during multidisciplinary sessions including radiologists, oncologists, and surgeons. Of 45 included patients, 5 were considered unresectable after NAC (2 patients had peritoneal carcinomatosis, 2 had lung and bone metastases, 1 had a contraindication for anesthesia) and were excluded from the cohort. The remaining 40 patients were scheduled for resection of CLMs by laparotomy including an intraoperative US.

All patients proved written informed consent. The study was approved by the institutional review board and the ethics committee of the State of Vaud.

Imaging Protocol

The mean interval between MRI and IV contrast-enhanced ¹⁸F-FDG PET/CT was 2.6 ± 4.5 days (range, 0–14 days). All examinations were performed at least 3 weeks after the end of NAC.

Liver MR examinations were acquired on a 3-T scanner (Skyra or Verio; Siemens, Erlangen, Germany). The technical parameters of MR sequences are reported in Table 1. The DW-MRI was performed before IV Gd-injection and included axial single-shot spin-echo echo-planar sequences in 3 orthogonal directions (frequency-encoding, phase-encoding, and slice-selection) with 3 b-values (50, 300, and 600 s/mm²). These b-values were chosen to obtain images with a sufficient contrast-to-noise ratio. Fat suppression was implemented by the SPAIR (spectral adiabatic inversion recovery) technique. Trace images were synthesized for each b-value, and an apparent diffusion coefficient (ADC) map was then automatically computed (with vendor-provided software) from all diffusion weightings and directions. The window width and level were set to adequately visualize the whole abdomen.

After acquiring an axial nonenhanced 3-dimensional (3D) volumetrical interpolation breath hold examination (VIBE) sequence, 0.1 mL/kg of Gd-EOB-DTPA was intravenously injected, followed by flushing with 40 mL of 0.9% NaCl saline. The 3D VIBE sequences centered on the upper abdomen were dynamically acquired (arterial, portal, and venous phases). Finally, additional axial and coronal 3D VIBE acquisitions were performed at the hepatobiliary phase, that is, 20 minutes after IV Gd-EOB-DTPA injection.

The ¹⁸F-FDG PET/CT examinations were performed on a Discovery LS or on a Discovery 690 PET/CT scanner (GE Healthcare, Milwaukee, WI). After fasting for at least 6 hours before the

examination, the blood glucose level was verified to be 8.3 mmol/L or less before administering ¹⁸F-FDG. Patients were then intravenously injected with 3.5 MBq/kg or 295 ± 70 MBq (range, 173–476 MBq) of ¹⁸F-FDG. A vertex to mid-thigh PET acquisition (2D mode with 6–8 steps of 3 minutes for the Discovery LS or 3D mode with 7–9 steps of 2 minutes for the Discovery 690; mean duration, 18 ± 2 minutes; range, 16–24 minutes) was performed 67 ± 9 minutes (range, 50–90 minutes) after IV administration of ¹⁸F-FDG. The PET data were reconstructed using an ordered-subset expectation maximization method with 8 subsets and 2 iterations. The PET acquisition was preceded by an upper abdominal contrast-enhanced multiple detector CT acquisition (16- or 64-row detector, 120 kV, automatic tube intensity modulation, pitch 1.5, 0.5 s/rotation, 2.5-mm reconstructed axial slice thickness) at the portal phase, that is, 70 seconds after IV injection of contrast media (Accupaque 300; GE Healthcare, 1 mL/kg of body weight, injection rate 2.5 mL/s followed by flushing with 40 mL of 0.9% NaCl saline). A second vertex to mid-thigh multiple detector CT acquisition (120 kV, 80 mA; pitch 1.5, 0.5 s/rotation, 5-mm slice thickness) at the excretory phase was used for attenuation correction. SUVs were corrected for body mass as previously reported.¹⁵

A radiologist (A.D.) with 20 years' experience in abdominal imaging performed the intraoperative US in the operating room, which served as a reference standard for the presence of CLM and was the basis for surgery.

Image Analysis

Image analysis included morphological assessment, a count of CLMs, and an evaluation of quantitative parameters derived from DW-MRI scans and ¹⁸F-FDG PET/CT.

Morphological analyses of MR and ¹⁸F-FDG PET/CT images were independently performed by 2 readers on 2 different workstations (Advantage; GE Healthcare, Milwaukee, WI). Each reader was blinded to the results of the second technique in a first reading phase. The MRI scans were analyzed by a first radiologist (S.S.) with 15 years' experience in abdominal imaging. The IV contrast-enhanced ¹⁸F-FDG PET/CT images were analyzed by a second reader (V.D.) with 10 years' experience as both a radiologist and nuclear medicine physician. On MRI scans, CLMs were defined according to previously published criteria for Gd-EOB-DTPA and DW-MRI.¹¹ On IV contrast-enhanced ¹⁸F-FDG PET/CT, CLMs were recorded as ¹⁸F-FDG-avid CLMs when they showed higher ¹⁸F-FDG uptake than the normal adjacent liver and were seen on IV contrast-enhanced CT, or as ¹⁸F-FDG non-avid when they

TABLE 1. Technical Parameters of MR Sequences

| Sequences | TR/TE, ms | Flip Angle, degrees | Pixel Size, mm | NEX | No. Slices Per Slab | Slice Thickness, mm | Parallel Imaging (iPAD) | Respiratory Method | Acquisition Time, min |
|--------------------------|-----------|---------------------|----------------|-----|---------------------|---------------------|-------------------------|------------------------|-----------------------|
| T2 HASTE axial | 1600/96 | 160 | 1.3 × 1.3 | 1 | 50 | 3 | GRAPPA 2 | Breath hold | 1.40 |
| T2 HASTE coronal | 1200/92 | 160 | 1.6 × 1.6 | 1 | 50 | 4 | GRAPPA 2 | Breath hold | 1.20 |
| T2 Turbo-spin-echo axial | 2220/70 | 90 | 0.5 × 0.5 | 2 | 36 | 5 | GRAPPA 2 | Respiratory gating | 2.15 |
| DWI SPAIR axial | 7700/66 | 90 | 3.5 × 2.8 | 6 | 30 | 6 | GRAPPA 2 | Free shallow Breathing | 7.20 |
| 3D VIBE axial | 3.62/1.32 | 10 | 1.8 × 1.5 | 1 | 92 | 2 | GRAPPA 2 | Breath hold | 0.22 |
| 3D VIBE coronal | 5.21/1.57 | 13 | 1.9 × 1.8 | 1 | 96 | 2 | GRAPPA 3 | Breath hold | 0.22 |

HASTE, half Fourier acquisition single-shot turbo spin-echo; DWI, diffusion-weighted imaging; SPAIR, spectral adiabatic inversion recovery fat suppression; NEX, number of excitations; iPAD, integrated parallel acquisition technique; GRAPPA, generalized autocalibrating partially parallel acquisitions.

Downloaded from http://online.lww.com/nucmed by BnDMSepHKAVT zeoumtIQINahHJLnEzgsiHd4XMI0hCy WCX1AWMYOpIQIHID33D000RyVTYSFIACI3VCYoaogqOZXdinHKZB7iws= on 03/20/2023

were not seen on PET images but appeared as ill-defined, low-density lesions on IV contrast-enhanced CT. The number, size, and the anatomical location of each metastasis were exactly registered for both imaging modalities.

To assess quantitative parameters of DW-MRI scans, a volume of interest (VOI) encompassing the whole lesion was manually drawn on DW-MRI scans around each CLM that was equally visible on the hepatobiliary phase of Gd-EOB-DTPA-enhanced MRI. To measure the corresponding mean and minimum ADCs (ADC_{mean} and ADC_{min}), the VOI was then copied and pasted on the corresponding ADC map. On IV contrast-enhanced ^{18}F -FDG PET/CT images, a 42% SUV_{max} threshold VOI was drawn around all recorded CLMs visible either on the ^{18}F -FDG PET (^{18}F -FDG-avid lesions, Fig. 1) or only on the enhanced CT (^{18}F -FDG non-avid lesions). The SUV_{max} , SUV_{mean} , metabolic tumor volume (MTV), and total lesion glycolysis (TLG) were measured. Using a 1-cm³ VOI placed in another liver segment without CLMs, the SUV_{mean} was used to calculate maximal and mean target-to-background ratios (TBR_{max} and TBR_{mean}). In case of overlapping lesions or when the distance between 2 adjacent CLMs was less than 1 cm, DW-MRI and ^{18}F -FDG PET-derived metrics were not measured to avoid possible overlap.

Histopathological Analysis

All the resected liver specimens were fixed in formalin. Representative sections of each CLM were embedded in paraffin, stained with hematoxylin and eosin, and then prospectively analyzed by 1 pathologist with more than 10 years' experience in liver pathology (C.S.), who was blinded to all the imaging results. Tumor regression grading (TRG; range, 1–5) was recorded on a “per-lesion” basis according to Rubbia-Brandt et al.¹⁶ Tumor regression grading included evaluation of tumor viability (TV; range, 0%–100%) that was graded according to the percentage of the whole CLM surface occupied by tumor cells. For tumor response characterization, the following criteria were considered: TRG 1 to 2 indicated major or complete histological response (ie, TV less

than 25%), TRG 3 indicated partial response (ie, TV of 25%–50%), and TRG 4 to 5 indicated (nearly) no histological response (ie, TV of >50%).¹⁶

Statistical Analysis

All statistical tests were performed with Stata 13.1 software. Continuous variables are presented as mean \pm standard deviation (SD) or as the median (interquartile range [IQR]). The Kruskal-Wallis and Wilcoxon signed rank tests were used to evaluate the number of metastases detected by each technique, always in comparison with intraoperative US, the standard reference. Second, we assessed the relationship between TV and the ADC and SUV resulting from DW-MRI or ^{18}F -FDG PET metrics, respectively. Each resected metastasis was matched with the lesion localization from intraoperative US to perform a per-lesion analysis. This relationship was assessed with linear regression analysis (r).

The resected lesions that could be quantitatively analyzed were divided into 2 groups according to their median size (<2.2 cm or \geq 2.2 cm). The Wilcoxon signed rank test was used to compare TV, as well as the DW-MRI and ^{18}F -FDG PET metrics between the 2 groups and according to the types of NAC (with or without targeted therapy).

A P value less than 0.05 was considered statistically significant for simple testing. For multiple testing, the significance level was corrected using the Bonferroni method.

RESULTS

Study Population

In the 40 operated patients, the combined Gd-EOB-DTPA-enhanced and DW-MRI and IV contrast-enhanced ^{18}F -FDG PET/CT were successfully performed and analyzed. The mean delay between imaging data acquisition and surgical resection was 18 ± 22 days (range, 2–102 days). Patients' characteristics are summarized in Table 2.

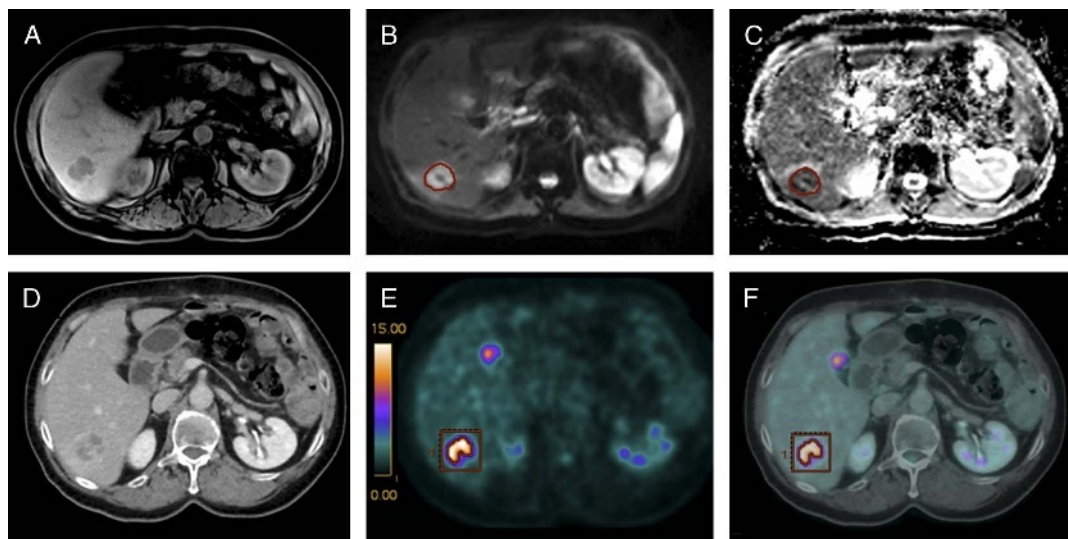


FIGURE 1. Colorectal liver metastasis (CLM) located in segment VI. The CLM appears as a 2.9-cm, hypointense, well-defined lesion on the late hepatobiliary phase axial MRI scan (A), as hyperintense on the DW MRI scan ($b = 600$) (B), and hypointense on the ADC map (C). On PET/CT, it is characterized as an ill-defined lesion with peripheral enhancement on the IV contrast-enhanced axial CT image (D) showing high ^{18}F -FDG uptake on PET and PET/CT fusion images (E and F). For this lesion, the 42% SUV_{max} threshold VOI indicates an SUV_{mean} of 12.0 g/mL and TBR_{mean} of 5.5 (E and F). The VOI delineated on DW images and copied and pasted on the correspondent ADC map (C) shows an ADC_{mean} of 1024×10^{-6} mm²/s. Histological analysis demonstrates the TV was 90% and tumor regression grade was 5.

TABLE 2. Patients' Characteristics

| Variables (n = 45) | Mean ± SD or n (%) |
|--------------------------------------|--------------------|
| Age, y | 63 ± 10 |
| Sex (n = 45) | |
| Male | 29 (64) |
| Female | 16 (36) |
| CLMs (n = 45) | |
| Synchronous | 28 (62) |
| Metachronous | 17 (38) |
| Surgery (n = 40) | |
| Hepatectomy | 9 (23) |
| Metastectomy/wedge resection | 31 (77) |
| Preoperative chemotherapy (n = 45) | |
| FOLFOX | 30 (67) |
| FOLFIRI | 11 (25) |
| FOLFOXIRI | 1 (2) |
| XELOX | 1 (2) |
| XELODA | 2 (4) |
| Without targeted therapy | 23 (51) |
| With targeted therapy | 22 (49) |
| Cetuximab (Erbixub) | 8 (18) |
| Bevacizumab (Avastin) | 14 (31) |
| No. CLMs per patient (n = 38) | |
| Intraoperative US | 4.0 ± 2.9 |
| Gd-EOB-DTPA-enhanced/DW-MRI | 3.8 ± 3.1 |
| IV contrast-enhanced PET/CT | 3.8 ± 4.4* |
| Delay between surgery and imaging, d | 18 ± 22 |

*P = 0.61 when comparing the 3 techniques (Kruskal-Wallis test).

Histological Findings

Forty patients underwent surgical resection of 122 lesions. Forty-eight resected CLMs were located in the left liver lobe and 74 in the right liver lobe. The mean lesion size was 1.9 ± 1.5 cm (median, 1.5 cm [IQR, 0.8–2.4]; range, 0.6–10.4 cm). Thirty-five (29%) CLMs were less than 1 cm and 87 (71%) 1 cm or greater. Histologically, 112 CLMs corresponded to a colorectal adenocarcinoma, 4 to adenosquamous CRC and 6 to mucinous colorectal adenocarcinoma. Sixty-two lesions showed no histological response (TRG 4–5, TV >50%), 34 lesions had a partial response (TRG 3, TV = 25%–50%) and 26 lesions had a major response (TRG 1–2,

TV <25%). The TV was not statistically significantly different for lesions treated with and without targeted NAC (51% ± 29%, n = 75 vs 54% ± 26%, n = 47, P = 0.58).

Imaging Results

Intraoperative US was performed in 38 of the 40 operated patients. It revealed 153 CLMs (mean size, 1.8 ± 1.1 cm; median, 1.5 [IQR, 1.0–2.4]; range, 0.5–10.4 cm), of which, 122 were resected. The detection rates of MRI (n = 147, 96%) and IV contrast-enhanced ¹⁸F-FDG PET/CT (n = 145, 95%) were similar (Table 2, P = 0.61), when compared with intraoperative US.

For 53 of the 122 resected CLMs, quantitative metrics were not recorded due to overlap between the lesions. The quantitative analysis resulting from the ¹⁸F-FDG PET and DW-MRI for the remaining 69 lesions has been summarized in Table 3. Metrics were not significantly influenced by the size of lesions (P ≥ 0.009) except for MTV and TLG (P = 0.001). There was no significant difference between patients who underwent NAC with or without targeted therapy (P ≥ 0.13). The SUV_{max} and ADC_{min} values were significantly negatively correlated (r = -0.34, P = 0.005) but not the SUV_{mean} and ADC_{mean} (r = -0.22, P = 0.09).

Radiopathological Correlation

The quantitative radiopathological correlation was performed on a per-lesion basis and included 69 of the 122 resected CLMs (mean size, 2.7 ± 1.6 cm; median, 2.2 [IQR, 1.7–3]; range, 0.6–10.4 cm). Thirty-six had no histological response (TRG 4–5), 24 had a partial response (TRG 3), and 9 had a major response (TRG 1–2). The TV was not different between lesions less than 2.2 cm and those 2.2 cm or greater (57.9% ± 26.8% vs 54.1% ± 20.5%, P = 0.27) or between lesions treated with and without targeted NAC (54.3% ± 23.0% vs 57.4% ± 24.1%, P = 0.66). The correlations between quantitative metrics resulting from ¹⁸F-FDG PET or DW-MRI and TV, as assessed on histological specimens, are displayed in Table 4. Only TBR_{max} and TBR_{mean} were significantly correlated with TV (r = 0.33, P = 0.006 and r = 0.37, P = 0.002, respectively).

DISCUSSION

Our study yielded 2 main results. First, the diagnostic value of combined Gd-EOB-DTPA-enhanced and DW-MRI was similar to IV contrast-enhanced ¹⁸F-FDG PET/CT, when compared with intraoperative US for the detection of CLMs after NAC, and second, TV was correlated with the TBR_{mean} and TBR_{max}, but not with ADC values, regardless of the type of NAC. These results extend

TABLE 3. ¹⁸F-FDG PET/CT and DW-MRI—Quantitative Analysis

| Metrics | All Lesions, n = 69 | Lesions <2.2 cm, n = 31 | Lesions ≥2.2 cm, n = 38 | P | With Targeted Therapy, n = 33 | Without Targeted Therapy, n = 36 | P |
|---|---------------------|-------------------------|-------------------------|--------|-------------------------------|----------------------------------|------|
| SUV _{max} , g/mL | 8.1 ± 4.1 | 6.8 ± 3.5 | 9.1 ± 4.3 | 0.023 | 8.0 ± 4.7 | 8.1 ± 3.5 | 0.61 |
| SUV _{mean} , g/mL | 4.8 ± 2.4 | 4.1 ± 2.0 | 5.4 ± 2.6 | 0.043 | 4.8 ± 2.7 | 4.9 ± 2.1 | 0.48 |
| TBR _{max} (1) | 3.3 ± 1.8 | 2.8 ± 1.5 | 3.8 ± 1.9 | 0.009 | 3.3 ± 2.1 | 3.4 ± 1.4 | 0.27 |
| TBR _{mean} (1) | 2.0 ± 1.1 | 1.7 ± 0.9 | 2.2 ± 1.1 | 0.022 | 2.0 ± 1.2 | 2.0 ± 0.9 | 0.13 |
| MTV, mL | 18.1 ± 19.9 | 10.1 ± 8.6 | 24.6 ± 23.9 | 0.001* | 21.1 ± 24.8 | 15.4 ± 13.9 | 0.51 |
| TLG, g | 83.2 ± 122.9 | 36.1 ± 25.5 | 121.6 ± 154.5 | 0.001* | 98.7 ± 164.9 | 68.9 ± 63.7 | 0.99 |
| ADC _{min} , 10 ⁻⁶ mm ² /s | 675 ± 308 | 697 ± 287 | 657 ± 328 | 0.37 | 610 ± 280 | 732 ± 323 | 0.16 |
| ADC _{mean} , 10 ⁻⁶ mm ² /s | 1260 ± 275 | 1264 ± 253 | 1255 ± 297 | 0.65 | 1245 ± 237 | 1272 ± 307 | 0.91 |

*Statistical significance after Bonferroni correction for multiple testing (P < 0.00625).

P values are given for comparison between lesions <2.2 cm and ≥2.2 cm or between lesions treated by NAC with or without targeted therapy using the Wilcoxon signed rank test.

Downloaded from http://jnm.sagepub.com at National Institute of Health on 03/20/2013

TABLE 4. Correlation Between DW-MRI, ¹⁸F-FDG PET Metrics, and TV (n = 69)

| Metrics | r | P |
|---|-------|--------|
| SUV _{max} , g/mL | 0.24 | 0.048 |
| SUV _{mean} , g/mL | 0.28 | 0.021 |
| TBR _{max} (1) | 0.33 | 0.006* |
| TBR _{mean} (1) | 0.37 | 0.002* |
| MTV, mL | -0.29 | 0.014 |
| TLG, g | -0.14 | 0.26 |
| ADC _{min} , 10 ⁻⁶ mm ² /s | -0.02 | 0.9 |
| ADC _{mean} , 10 ⁻⁶ mm ² /s | 0.01 | 0.9 |

*Statistical significance after Bonferroni correction for multiple testing ($P < 0.00625$).

our knowledge of the 2 main roles of imaging of CLMs after NAC, namely, the detection of residual lesions and the assessment of tumor response.

Supporting our results of CLM detection, most recent studies demonstrated that combined Gd-EOB-DTPA-enhanced and DW-MRI improved detection performance compared with enhanced CT,⁹ or each MR technique alone.^{10,11,17} Our finding of a similar detection rate of combined Gd-EOB-DTPA-enhanced and DW-MRI to IV contrast-enhanced ¹⁸F-FDG PET/CT implies that IV contrast media injection should be mandatory when using ¹⁸F-FDG PET/CT for the detection of CLMs after NAC.¹⁸ Our results also agree with the findings of Seo et al¹⁹ who demonstrated similar performances for Gd-EOB-DTPA-enhanced MRI and contrast-enhanced ¹⁸F-FDG PET/CT for lesions greater than 1 cm, which represented two thirds (n = 80) of the resected lesions in our study. For lesions 1 cm or less, the same authors found that Gd-EOB-DTPA-enhanced MRI was more accurate than contrast-enhanced ¹⁸F-FDG PET/CT.¹⁹ In contrast, we did not find a significant difference in the detection rate between MRI and contrast-enhanced ¹⁸F-FDG PET/CT for lesions 1 cm or less (n = 42) in this study (100% vs 98%, $P = 0.35$). Thus, when dealing only with the preoperative detection of CLMs after NAC and resection planning,²⁰ combined Gd-EOB-DTPA-enhanced and DW-MRI is preferred over other imaging techniques to limit the patients' radiation exposure. In patients with a MRI contraindication, contrast-enhanced ¹⁸F-FDG PET/CT is a valuable alternative. Nevertheless, when patients are judged resectable, intraoperative US is mandatory,²¹ especially in fatty livers,²² to ensure accurate localization of the tiniest lesions. However, it does not assess TV.

Evaluating the tumor response to NAC is the second aim of preoperative imaging. Morphologically, this is usually reported as shrinkage of the size of CLMs size; although according to Rubbia-Brandt et al,¹⁶ the lesion's diameter is not significantly correlated with the TRG. Therefore, metabolic information is needed. This has traditionally been obtained by ¹⁸F-FDG PET/CT; however, during the last decade, DW-MRI has also been used in this regard.¹⁵ Our results demonstrated a significant correlation of TBR_{max} and TBR_{mean} with TV on a per-lesion basis. This is in agreement with a previous study by Burger et al,¹² who showed that the relative change in ¹⁸F-FDG avidity of CLMs after NAC correlated with TRG. They also confirmed the usefulness of ¹⁸F-FDG PET metrics for the evaluation of the viability and metabolic response of CLMs after NAC, which correlated with longer overall and progression-free survival.^{23,24} In contrast, our quantitative analysis of DW-MRI scans did not reveal any significant correlation between the ADC values and the corresponding TV. Few studies have been published on this

topic, despite the proven good reproducibility of iterative ADC measurements.²⁵ Two studies suggested that changes in DW-MRI-related parameters²⁶ and histograms derived from ADC maps²⁷ could help predict the response to chemotherapy. However, these authors had no histological confirmation regarding TV and used RECIST 1.1 size criteria, which are poorly correlated with the histopathological response of CLMs.²⁸ Recently, Wagner et al²⁹ found that global ADC values, when including the entire lesion surface, measured in an ellipsoid region of interest (ROI) taken on the equatorial plane of the tumor did not help predict tumor response. We found the same results after measuring global ADC values, however, including the entire tumor volume. Wagner et al²⁹ also noted that in lesions larger than 1 cm, the ADC values measured in the tumor periphery were higher in cases with a major histological response; thus, suggested peripheral ADC measurements may be useful in identifying major responding CLMs. However, these authors limited their ADC measurements to a single ROI on a single tumor slice, unlike our study that included VOI measurements encompassing the whole CLM. Therefore, the impact of the location of the peripheral ROIs and the consecutive measurement variability due to tumor heterogeneity remain unclear.

Our results revealed that the SUV_{max} and ADC_{min} values of the 69 CLMs were negatively correlated ($r = -0.34$, $P = 0.005$) on preoperative imaging after NAC, but not the SUV_{mean} and ADC_{mean}. This statistically significant correlation between SUV_{max} and ADC_{min} perfectly agrees with previous oncological imaging studies.^{15,30,31} Schmidt et al¹⁵ had even demonstrated a significant association between changes in SUV_{max} and ADC_{min} ($P = 0.0014$) when assessing the response of metastatic GIST to targeted therapy.

In the setting of the development of hybrid imaging, especially PET/MRI, only few publications deal with CLMs. Donati et al³² demonstrated that the retrospective fusion of ¹⁸F-FDG PET and MRI scans performed similarly to Gd-EOB-DTPA-enhanced MRI for the detection of liver metastases of various primary cancers, including CRC. More recently, Lee et al³³ found that the diagnostic value of ¹⁸F-FDG PET/MRI was similar to that of Gd-EOB-DTPA-enhanced MRI for the detection of CLMs. Focusing on a small subgroup of 18 patients (33% of the study population) who underwent NAC before surgery, these authors also showed that patients with isometabolic CLMs after NAC had a better recurrence-free survival than patients with hypermetabolic CLMs after NAC. They concluded that ¹⁸F-FDG PET/MRI yields both high diagnostic and prognostic information. Thus, our results and those from previous studies suggest that ¹⁸F-FDG PET/MRI including combined Gd-EOB-DTPA-enhanced and DW sequences could provide optimal preoperative detection of CLMs after NAC and accurate characterization of tiny lesions, whereas reducing patients' dose exposures from CT. The use of ¹⁸F-FDG PET metrics (ie, TBR_{max} and TBR_{mean}) would simultaneously assess the tumor's metabolic response, which reflects the TRG and TV and is an indicator of the patient's prognosis. However, when MRI is contraindicated, contrast-enhanced ¹⁸F-FDG PET/CT remains a valuable alternative.

Some limitations of our study have to be addressed. First, we enrolled patients who underwent various NAC protocols, with about half undergoing additional targeted therapy. However, TV, and the DW-MRI and ¹⁸F-FDG PET metrics were not different between lesions treated with and without targeted therapy. This suggests that the heterogeneity of NAC protocols may not account for a confounding factor in our analysis. Second, PET acquisitions were performed on 2 different scanners with slightly different transverse spatial resolutions (5.8 mm for Discovery LS and 4.7 mm for Discovery HD 690, difference 1.1 mm). Third, only 69 of 122 resected CLMs (57%) could be quantitatively correlated to pathological findings. However, by excluding overlapping lesions, we could avoid possible measurement errors on DW-MR and PET images.

Finally, DW-MRI and ^{18}F -FDG PET-derived parameters were measured on 2 different scanners; thus, it would be of interest to confirm our results on a hybrid PET/MRI scanner.

Finally, we did not include the findings of pretherapy imaging in our evaluation, because our patients were addressed to our University Hospital for NAC and subsequent surgery of their metastatic liver disease after an initial evaluation in a peripheral secondary health care center. Therefore, pretherapy examinations had been performed on different MR and PET/CT machines than ours and the difference in acquisition parameters would have hampered the comparison between pretherapy and posttherapy imaging.

In conclusion, while both combined Gd-EOB-DTPA-enhanced and DW-MRI, and IV contrast-enhanced ^{18}F -FDG PET/CT allow confident detection of residual CLMs, only ^{18}F -FDG PET metrics are able to predict TV after NAC. This suggests there is high diagnostic and prognostic potential for hybrid ^{18}F -FDG PET/MRI, but this would need to be evaluated by future studies.

REFERENCES

1. Ferlay J, Soerjomataram I, Dikshit R, et al. Cancer incidence and mortality worldwide: sources, methods and major patterns in GLOBOCAN 2012. *Int J Cancer*. 2015;136:E359–E386.
2. Scheele J, Stangl R, Altendorf-Hofmann A. Hepatic metastases from colorectal carcinoma: impact of surgical resection on the natural history. *Br J Surg*. 1990;77:1241–1246.
3. Kanas GP, Taylor A, Primrose JN, et al. Survival after liver resection in metastatic colorectal cancer: review and meta-analysis of prognostic factors. *Clin Epidemiol*. 2012;4:283–301.
4. Fong Y, Cohen AM, Fortner JG, et al. Liver resection for colorectal metastases. *J Clin Oncol*. 1997;15:938–946.
5. Ruers T, Bleichrodt RP. Treatment of liver metastases, an update on the possibilities and results. *Eur J Cancer*. 2002;38:1023–1033.
6. Adam R, de Gramont A, Figueras J, et al. Managing synchronous liver metastases from colorectal cancer: a multidisciplinary international consensus. *Cancer Treat Rev*. 2015;41:729–741.
7. Nuzzo G, Giulianti F, Ardito F, et al. Liver resection for primarily unresectable colorectal metastases downsized by chemotherapy. *J Gastrointest Surg*. 2007;11:318–324.
8. Zech CJ, Justo N, Lang A, et al. Cost evaluation of gadoxetic acid-enhanced magnetic resonance imaging in the diagnosis of colorectal-cancer metastasis in the liver: results from the VALUE Trial. *Eur Radiol*. 2016;26:4121–4130.
9. Kim HJ, Lee SS, Byun JH, et al. Incremental value of liver MR imaging in patients with potentially curable colorectal hepatic metastasis detected at CT: a prospective comparison of diffusion-weighted imaging, gadoxetic acid-enhanced MR imaging, and a combination of both MR techniques. *Radiology*. 2015;274:712–722.
10. Yu MH, Lee JM, Hur BY, et al. Gadoxetic acid-enhanced MRI and diffusion-weighted imaging for the detection of colorectal liver metastases after neoadjuvant chemotherapy. *Eur Radiol*. 2015;25:2428–2436.
11. Colagrande S, Castellani A, Nardi C, et al. The role of diffusion-weighted imaging in the detection of hepatic metastases from colorectal cancer: a comparison with unenhanced and Gd-EOB-DTPA enhanced MRI. *Eur J Radiol*. 2016;85:1027–1034.
12. Burger IA, Schwarz EI, Samarin A, et al. Correlation between therapy response assessment using FDG PET/CT and histopathologic tumor regression grade in hepatic metastasis of colorectal carcinoma after neoadjuvant therapy. *Ann Nucl Med*. 2013;27:177–183.
13. Lau LF, Williams DS, Lee ST, et al. Metabolic response to preoperative chemotherapy predicts prognosis for patients undergoing surgical resection of colorectal cancer metastatic to the liver. *Ann Surg Oncol*. 2014;21:2420–2428.
14. Xia Q, Liu J, Wu C, et al. Prognostic significance of (18)FDG PET/CT in colorectal cancer patients with liver metastases: a meta-analysis. *Cancer Imaging*. 2015;15:19.
15. Schmidt S, Dunet V, Koehli M, et al. Diffusion-weighted magnetic resonance imaging in metastatic gastrointestinal stromal tumor (GIST): a pilot study on the assessment of treatment response in comparison with ^{18}F -FDG PET/CT. *Acta Radiol*. 2013;54:837–842.
16. Rubbia-Brandt L, Giostra E, Brezault C, et al. Importance of histological tumor response assessment in predicting the outcome in patients with colorectal liver metastases treated with neo-adjuvant chemotherapy followed by liver surgery. *Ann Oncol*. 2007;18:299–304.
17. Vilgrain V, Esvan M, Ronot M, et al. A meta-analysis of diffusion-weighted and gadoxetic acid-enhanced MR imaging for the detection of liver metastases. *Eur Radiol*. 2016;26:4595–4615.
18. García Vicente AM, Domínguez Ferreras E, Sánchez Pérez V, et al. Response assessment of colorectal liver metastases with contrast enhanced CT/ ^{18}F -FDG PET. *Eur J Radiol*. 2013;82:e255–e261.
19. Seo HJ, Kim MJ, Lee JD, et al. Gadoxetate disodium-enhanced magnetic resonance imaging versus contrast-enhanced ^{18}F -fluorodeoxyglucose positron emission tomography/computed tomography for the detection of colorectal liver metastases. *Invest Radiol*. 2011;46:548–555.
20. Sofue K, Tsurusaki M, Murakami T, et al. Does Gadoxetic acid-enhanced 3.0 T MRI in addition to 64-detector-row contrast-enhanced CT provide better diagnostic performance and change the therapeutic strategy for the preoperative evaluation of colorectal liver metastases? *Eur Radiol*. 2014;24:2532–2539.
21. Arita J, Ono Y, Takahashi M, et al. Routine preoperative liver-specific magnetic resonance imaging does not exclude the necessity of contrast-enhanced intraoperative ultrasound in hepatic resection for colorectal liver metastasis. *Ann Surg*. 2015;262:1086–1091.
22. Berger-Kulemann V, Schima W, Baroud S, et al. Gadoxetic acid-enhanced 3.0 T MR imaging versus multidetector-row CT in the detection of colorectal metastases in fatty liver using intraoperative ultrasound and histopathology as a standard of reference. *Eur J Surg Oncol*. 2012;38:670–676.
23. De Bruyne S, Van Damme N, Smeets P, et al. Value of DCE-MRI and FDG-PET/CT in the prediction of response to preoperative chemotherapy with bevacizumab for colorectal liver metastases. *Br J Cancer*. 2012;106:1926–1933.
24. Mertens J, De Bruyne S, Van Damme N, et al. Standardized added metabolic activity (SAM) IN ^{18}F -FDG PET assessment of treatment response in colorectal liver metastases. *Eur J Nucl Med Mol Imaging*. 2013;40:1214–1222.
25. Heijmen L, Ter Voert EE, Nagtegaal ID, et al. Diffusion-weighted MR imaging in liver metastases of colorectal cancer: reproducibility and biological validation. *Eur Radiol*. 2013;23:748–756.
26. Kim JH, Joo I, Kim TY, et al. Diffusion-related MRI parameters for assessing early treatment response of liver metastases to cytotoxic therapy in colorectal cancer. *Am J Roentgenol*. 2016;W1–W7.
27. Liang HY, Huang YQ, Yang ZX, et al. Potential of MR histogram analyses for prediction of response to chemotherapy in patients with colorectal hepatic metastases. *Eur Radiol*. 2016;26:2009–2018.
28. Egger ME, Cannon RM, Metzger TL, et al. Assessment of chemotherapy response in colorectal liver metastases in patients undergoing hepatic resection and the correlation to pathologic residual viable tumor. *J Am Coll Surg*. 2013;216:845–856. discussion 856–847.
29. Wagner M, Ronot M, Doblas S, et al. Assessment of the residual tumour of colorectal liver metastases after chemotherapy: diffusion-weighted MR magnetic resonance imaging in the peripheral and entire tumour. *Eur Radiol*. 2016;26:206–215.
30. Barabasch A, Kraemer NA, Ciritzis A, et al. Diagnostic accuracy of diffusion-weighted magnetic resonance imaging versus positron emission tomography/computed tomography for early response assessment of liver metastases to Y90-radioembolization. *Invest Radiol*. 2015;50:409–415.
31. Heijmen L, Ter Voert EE, Oyen WJ, et al. Multimodality imaging to predict response to systemic treatment in patients with advanced colorectal cancer. *PLoS One*. 2015;10:e0120823.
32. Donati OF, Hany TF, Reiner CS, et al. Value of retrospective fusion of PET and MR images in detection of hepatic metastases: comparison with ^{18}F -FDG PET/CT and Gd-EOB-DTPA-enhanced MRI. *J Nucl Med*. 2010;51:692–699.
33. Lee DH, Lee JM, Hur BY, et al. Colorectal cancer liver metastases: diagnostic performance and prognostic value of PET/MR imaging. *Radiology*. 2016;280:782–792.